Bulgarian Chemical Communications, Volume 47, Special Issue B (pp. 423–432) 2015

Integrated multiscale modeling approach for hierarchical biological nanocomposites applied to lobster cuticle

S. Nikolov[1*], H. Fabritius[2], M. Friák[2], D. Raabe[2]

[1] *Institute of Mechanics, Bulgarian Academy of Sciences, Acad. G. Bontchev Str. Bl. 4, 1113 Sofia, Bulgaria*
[2] *Max-Planck-Institut für Eisenforschung GmbH, Max-Planck-Str. 1, 40237 Düsseldorf, Germany*

Biological structural materials (e.g., bone, arthropod cuticles, shells) are organic-inorganic nanocomposites with hierarchically organized microstructure. A powerful tool to obtain the structure/property relations in such materials is multiscale modeling encompassing all length scales. Here we present an integral multiscale modeling approach for computing and prediction of the elastic properties of mineralized biomaterials. We combine *ab initio* calculations using Density Functional Theory (DFT) at the atomistic scale, step-by-step homogenization modeling at the mesoscale, and full-field spectral method based on Fast Fourier Transforms (FFT) for the macroscopic scale. An essential part of the concept is the experimental input to the model concerning the material structure and composition. We apply our multiscale concept to the cuticle of lobster. The cuticle consists of chitin nanofibrils, proteins, and mineral nanoparticles, and contains numerous pore canals across its thickness. The elastic properties at each hierarchical level are estimated and compared to experimental data for dry cuticle. At the mesoscale, the properties of cuticle proteins are identified and the bulk mineralized tissue is investigated. We find that the Young's modulus of the bulk tissue along the chitin fibrils is $\sim 60\%$ larger compared the modulus in direction perpendicular to the fibrils. At the macroscale, the highest stress concentrations in the cuticle in uniaxial in-plane loadings appear in planes where: (i) the major axes of the ellipsoidal pores (as well as the chitin fibrils) are oriented at about $\pm 45^\circ$ w.r.t. the loading direction, (ii) the separation regions between the pores are thinnest, and (iii) the shear stresses in the separation regions are close to their maximal values. We suggest that these are the necessary conditions for damage initiation in the lobster cuticle.

Key words: structural modeling, mechanical properties of tissues, biomaterials, organic-inorganic nanostructures, computational techniques; simulations

INTRODUCTION

Structural biomaterials (e.g., the bones of vertebrates, the exoskeletons of arthropods, mollusk shells) are known to possess excellent mechanical properties, e.g., in terms of stiffness-to-density ratio and fracture toughness, despite the modest characteristics of their constituents [1]. From the viewpoint of materials science, these materials are organic-inorganic nanocomposites formed via self-assembly of structural biopolymers like collagen (vertebrates) or chitin (arthropoda), various proteins, and nanoscopic mineral particles. As a rule, the basic components are hierarchically organized over multiple levels from the molecular to the macroscopic scales [2].

In order to understand the design principles and the performance of structural biomaterials, it is necessary to study the relationship between their structure, composition and the resulting physical properties. A powerful approach allowing to obtain and analyze structure/property relations is multiscale modeling encompassing all length scales [3]. To set up a proper multiscale model, a detailed structural description based on experimental findings is necessary. Specifically at the nanoscale, however, experimental studies of biomaterials are rather challenging and many properties of basic constituents are still unknown. To overcome these difficulties, *ab initio* quantum mechanical calculations can be used to determine experimentally inaccessible materials characteristics.

Because of the complexity of biomaterials, as well as the very limited size of studied systems inherent to the *ab initio* method, a complementary combination of *ab initio* calculations with higher-scale hierarchical modeling based on continuum micromechanics of heterogeneous materials represents an optimum strategy [3, 4]. A reliable hierarchical modeling over all length scales can identify the most important parameters relevant to certain structure/property relations and the tolerance of the overall material behavior against structural variations [4]. Moreover, such modeling can be very useful for the design and the optimization of new biomimetic hierarchical materials [5].

Here we present a hierarchical modeling approach for computing and prediction of the elastic properties of mineralized biomaterials at all length scales. In our concept, we combine *ab initio* calculations

* To whom all correspondence should be sent:
sv.nikolov@imbm.bas.bg

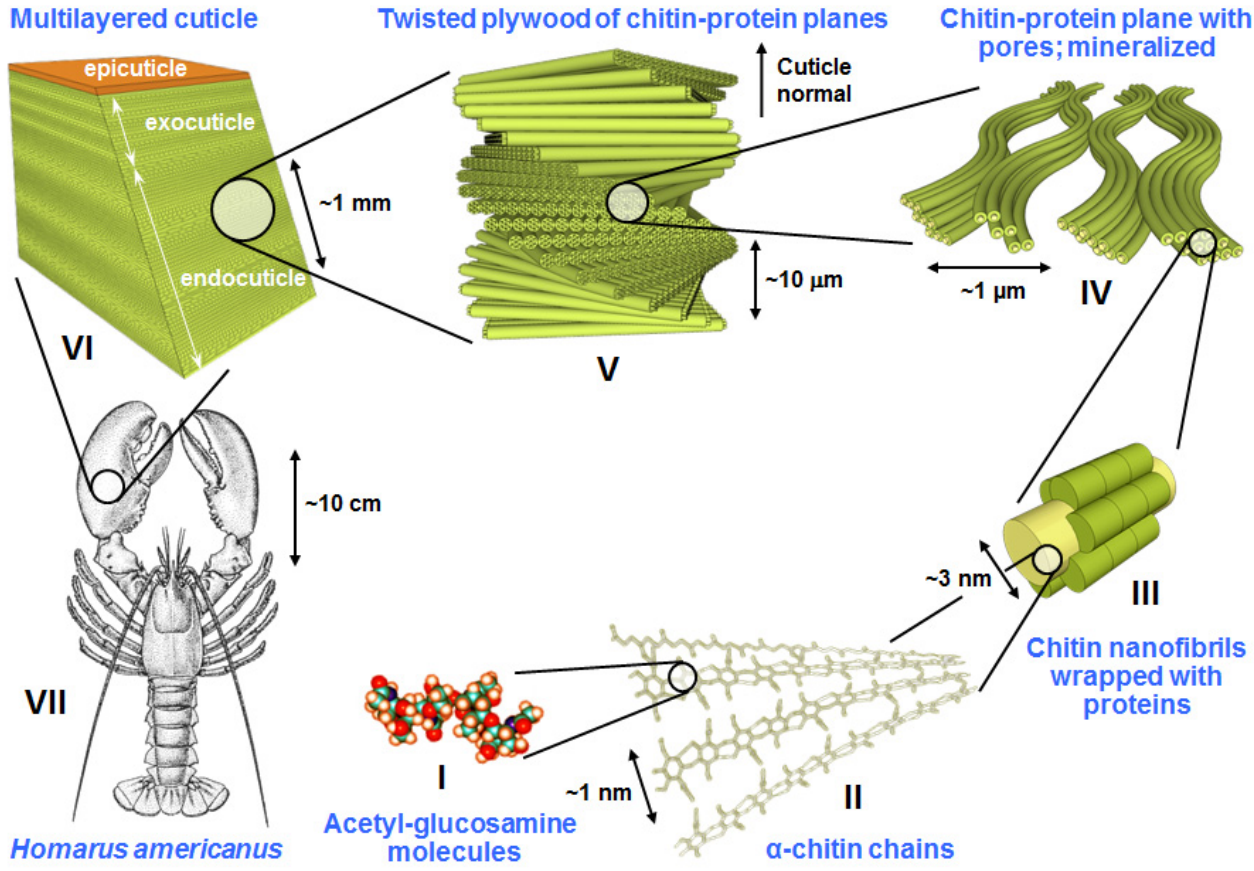

Fig. 1. Structural hierarchy of the cuticle of *Homarus americanus*. Mineral nanoparticles (levels IV, V, VI) and twisted ribbon-like pore canals (levels V, VI) are not visible.

using Density Functional Theory (DFT) at the nanoscale, step-by-step homogenization modeling at the mesoscale, and full-field spectral method based on Fast Fourier Transforms (FFT) for the macroscopic scale. The cuticle of a large marine crustacean, the lobster *Homarus americanus*, is chosen as a model material[1]. The necessary model input from experiments concerning the structure, the composition and the properties of the cuticle is obtained via different experimental techniques such as Scanning Electron Microscopy (SEM), Raman spectroscopy, X-ray diffraction, thermo-gravimetric analysis, nanoindentation, micro-tensile and micro-compression experiments [7–9].

The hierarchical structure of the mineralized lobster cuticle [4, 7, 8] is schematically shown in Fig. 1.

In Fig. 1, the lowest (nanoscale) hierarchical level is represented by N-acetyl-D-glucosamine molecules (I) which polymerize to form polysaccharide chains of chitin (II). At the next hierarchy level (III), 19 chitin chains arrange in anti-parallel pattern to form crystalline α-chitin nanofibrils [10] with diameter of $\sim 3\,\mathrm{nm}$ and length of $\sim 300\,\mathrm{nm}$. Each nanofibril is individually wrapped with proteins. Next, the chitin-protein fibrils cluster and associate with inorganic nanoparticles (mostly of amorphous calcium carbonate (ACC) [9]) and matrix proteins (see Fig. 2, III(b)) to form mineralized chitin-protein planes (IV). The wavy arrangement of the fibrils forms voids and gives the mineralized chitin-protein plane a honeycomb-like appearance. The individual planes (IV) are stacked over each other and gradually rotate around the normal direction of the cuticle, which results in a twisted plywood (Bouligand) structure (V) pierced by pore canals in the form of twisted ribbons with elliptical cross section. The stacking height (the distance

[1]The mineralized crustacean cuticle is the oldest (already present in the the Early Cambrian period ~ 515 Myr ago [6]) and one of the most successful natural materials for structural and armor applications produced by evolution.

in which a 180° rotation of superimposed planes is accomplished) of the twisted plywood in the endocuticle is $\sim 30\,\mu$m [8]. At the macroscale (VI), the cuticle consists of three layers: endocuticle, exocuticle, and a thin waxy epicuticle. The mechanically relevant exo- and endocuticle have the same basic microstructure but the mineral content in the exocuticle is higher and the pore canals are smaller. The stacking height in the exocuticle is $\sim 10\,\mu$m [8].

The main improvement of the present concept over our recently proposed model for crustacean cuticle [4] is in the modeling at the macroscopic scale. In [4], the twisted plywood geometry was approximated by honeycomb with thick walls and modeled via homogenization techniques. Here, the exact cuticle geometry taken from SEM micrographs (Fig. 2, V(exp.), V) is introduced in the model. The plywood mechanical behavior is computed via full-field FFT-based spectral method [11–13], which allows us to obtain and analyze the local stress and strain fields for different loadings. In contrast to our previous work dealing with wet cuticle, here we assess the properties of a dry cuticle. To refine our modeling and achieve better identification of the properties at the mesoscale, we use data from nanoindentation experiments [7] which can be properly performed only on dry cuticle.

Throughout the paper, notation is as follows: tensors without explicitly written indices are in boldface, the tensor product contracted over two indices is denoted by (:), tensor product is indicated by ($\otimes$), the inverse of a matrix (fourth-order tensors are in matrix representation because of symmetries) is denoted by $(\bullet)^{-1}$.

INTEGRATED MULTISCALE MODELING APPROACH

The multiscale hierarchical modeling of the cuticle is depicted in Fig. 2.

The main goal is to obtain the elastic constants of the cuticle (a fundamental characteristic of any het-

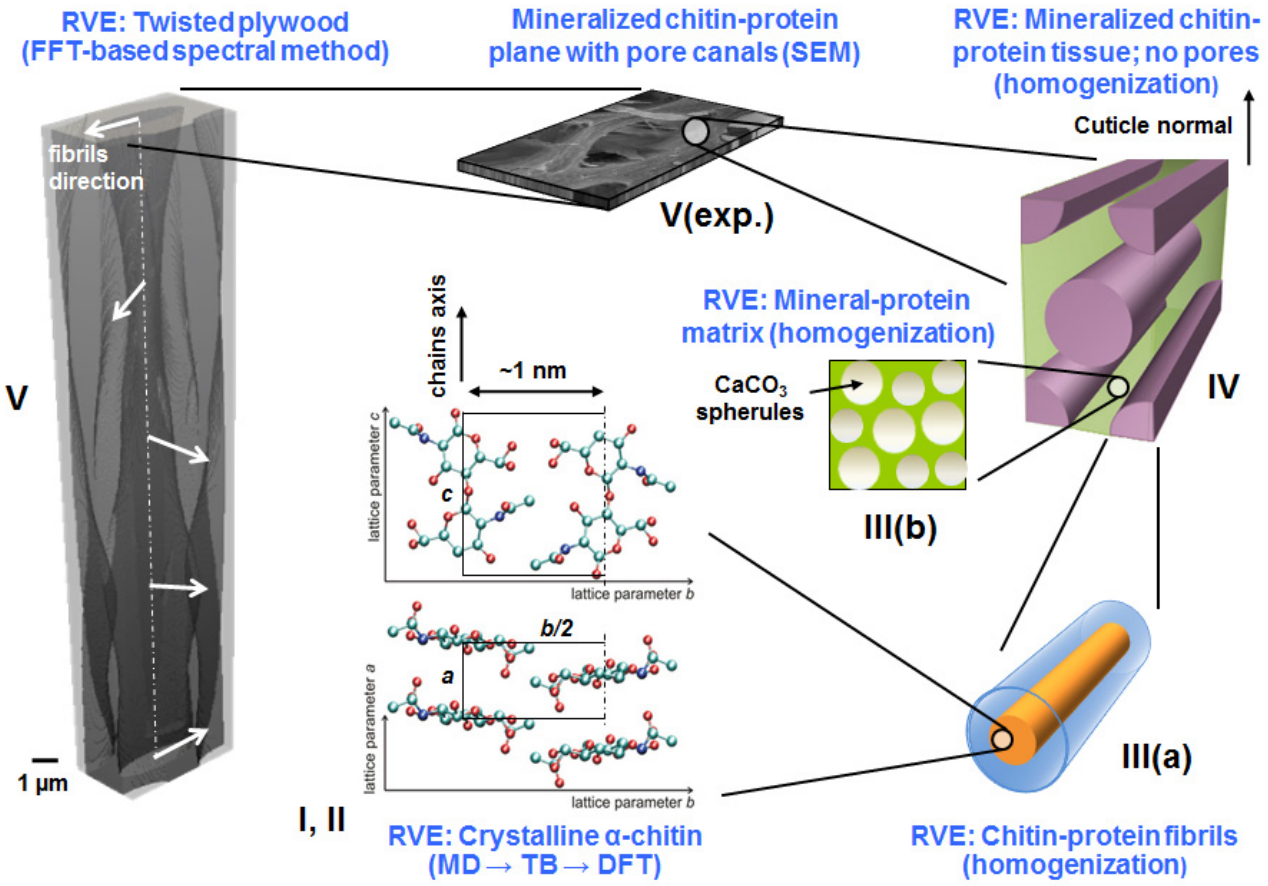

Fig. 2. Multiscale hierarchical modeling of the cuticle and methods used at different length scales.

erogeneous body) at each hierarchy level and corresponding length scale as a function of the underlying structure, composition, and the properties of the individual components. The information is passed from lower to upper hierarchy level of the model in a 'handshaking' manner. For example, the elastic constants of chitin obtained from *ab initio* calculations (Fig. 2, I,II) are directly introduced in a continuum-scale model to find the stiffness tensor of the chitin-protein fibrils (Fig. 2, III(a)). It is noted that the input from precise experimental measurements is an essential part in our integrated approach. For example, the Representative Volume Element (RVE) for the FFT-based calculations is constructed such that it matches as closely as possible the ensemble of the corresponding SEM micrographs (Fig. 2, V(exp.), V).

Ab initio modeling of α-chitin at the nanoscale

Because of the extremely small length scale and the difficulty to obtain a pure α-chitin sample, it is nearly impossible to experimentally measure the 3D elastic constants of the crystalline α-chitin nanofibrils (see Fig. 1, III). We used *ab initio* calculations to find the ground state atomic geometry and the stiffness tensor of the α-chitin crystal (for more details, see [4] and the references therein). Obtaining the atomic configuration of chitin is a rather challenging task because the exact positions of the hydrogen atoms and the number of hydrogen bonds are not directly accessible by experimental X-rays analysis. Moreover, the side groups ($-$OH, $-CH_2OH$, and $-NHCOCH_3$) of the chitin chains exhibit high structural flexibility. To tackle these difficulties we use a hierarchical approach using Valence Force Field Molecular Dynamics (VFFMD), Tight Binding (TB) and Density functional Theory (DFT) calculations.

As a first step, VFFMD simulations with probabilistic conformational search are performed. Starting from a rather arbitrary atomic geometry that conserves the chemical formula of α-chitin, an extended room temperature molecular-dynamics run sampled the multi-dimensional Born-Oppenheimer surface. Based on the criteria of minimum potential energy and maximum hydrogen bonds, about 10^2 out of 10^5 simulated structures emerged as likely. In a second step, the properties of the thus chosen configurations have been refined and re-checked employing self-consistent Density Functional Tight Binding (DFTB) calculations. About 10 low-energy structures emerged from the DFTB calculations and have been used as input to the subsequent DFT parameter-free calculations based on quantum mechanics.

The final result for the ground-state structure of crystalline α-chitin is shown in Fig. 2, I,II [4]. It has an orthorhombic unit cell with unit vectors a, b, and c[2]. The resulting lattice constants agree within 5% with the experimentally measured ones [14]. The corresponding stiffness tensor, $\mathbf{C}_{CH}$, was determined from the response of the chitin crystal on uniaxial stresses applied along the unit cell vectors a, b and c [4].

Homogenization modeling for hierarchy levels at the mesoscale

A classical problem in solid mechanics is the determination of the effective fourth-order stiffness tensor, $\mathbf{C}_e$, of a heterogeneous material consisting of inclusions embedded in a matrix. In elasticity, the goal of homogenization is to find $\mathbf{C}_e$ as a function of the microstructure so that a generalized Hooke's law holds:

$$\langle \boldsymbol{\sigma}(\mathbf{x}) \rangle = \mathbf{C}_e : \langle \boldsymbol{\varepsilon}(\mathbf{x}) \rangle \qquad (1)$$

where $\boldsymbol{\sigma}(\mathbf{x})$ and $\boldsymbol{\varepsilon}(\mathbf{x})$ are the second-order local stress and strain tensors, respectively; angular brackets denote ensemble average.

To solve the problem, one defines a Representative Volume Element (RVE), which is generally much smaller than the studied body but large enough to contain the same statistical information about the microstructure as the body itself. To compute $\mathbf{C}_e$, various mean-field homogenization models were developed (see, e.g., [15]). They assume that the stress and strain fields in the matrix and in the inclusions are adequately represented by their volume-averaged values. These models are limited to ellipsoidal inclusions and use as microstructural information the properties and the volume fractions of the phases, shape (but not dimensions) and orientations of the inclusions.

A different homogenization method has been developed by Torquato [16]. It consists in exact perturbation series expansion for the effective stiffness tensor, $\mathbf{C}_e$, of macroscopically anisotropic composite with two isotropic phases. This method is valid for arbitrary volume fractions and contrast between the phase properties. It also accounts for the specific arrangement of the inclusions (of arbitrary shape) via 3-

[2] The c (chain) direction of the α-chitin crystal coincides with the axis of the chitin nanofibrils (Fig. 1, III; Fig. 2, III(a)).

point statistical correlation parameters. The Torquato 3-point estimates are restricted to composites with two isotropic phases and have been specialized for 2D and 3D macroscopically isotropic composites [17].

Firstly, we derive the effective properties of the chitin-protein fibrils employing the Mori-Tanaka homogenization scheme [18, 19]. The RVE of a single chitin-protein fibril is shown in Fig. 2, III(a). Its homogenized stiffness tensor, $\mathbf{C}_F$, depends on the α-chitin stiffness tensor, $\mathbf{C}_{CH}$ (obtained through *ab initio* calculations), and the stiffness tensor of the surrounding protein matrix, $\mathbf{C}_{FP}$. The Mori-Tanaka estimate for $\mathbf{C}_F$ reads:

$$\mathbf{C}_F = \mathbf{C}_{FP} + \phi_{CH}[(\mathbf{C}_{CH} - \mathbf{C}_{FP}):\mathbf{A}_{CH}][(1-\phi_{CH})\mathbf{I} + \phi_{CH}\mathbf{A}_{CH}]^{-1} \quad (2)$$

where

$$\mathbf{A}_{CH} = [\mathbf{I} + \mathbf{S}_{CH}:(\mathbf{C}_{FP})^{-1}:(\mathbf{C}_{CH} - \mathbf{C}_{FP})]^{-1} \quad (3)$$

is the strain concentration factor for a chitin ellipsoidal inclusion in an infinite protein matrix; $\mathbf{I}$ is the fourth-order identity tensor; $\mathbf{S}_{CH}$ is the fourth-order Eshelby's tensor depending only on the shape of the inclusions and the elastic constants of the matrix (see, e.g., [15]); ϕ_{CH} is the volume fraction of the chitin nanofibril.

Next, from experimental evidence, the mineral-protein matrix is modeled as an isotropic composite of packed $CaCO_3$ spheres embedded in a protein matrix (Fig. 2, III(b)). Because of the very high volume fraction of the mineral spheres (the mineral content is $\sim 70\,\%$ of the weight of a wet cuticle) and the strong contrast between the mineral and protein properties, we use the Torquato 3-point estimates for the bulk and shear moduli. Let phases 1 and 2 with volume fractions ϕ_1 and $\phi_2 = 1 - \phi_1$ denote the protein matrix and the mineral particles, respectively. With K_1, K_2 being the bulk, and G_1, G_2 the shear moduli of the matrix and the inclusions, respectively, the effective bulk, K_M, and shear, G_M, moduli of the mineral-protein matrix read [17]:

$$K_M = K_1 \left(\frac{1 + \frac{4G_1}{3K_1}\kappa\phi_2 - \frac{10G_1}{3(K_1+2G_1)}\kappa\mu\phi_1\zeta_2}{1 - \kappa\phi_2 - \frac{10G_1}{3(K_1+2G_1)}\kappa\mu\phi_1\zeta_2} \right) \quad (4)$$

$$G_M = G_1 \left(\frac{1 + \frac{9K_1+8G_1}{6(K_1+2G_1)}\mu\phi_2 - \frac{2\kappa\mu G_1}{3(K_1+2G_1)}\phi_1\zeta_2 - \frac{\mu^2}{6}\left\{ \left[\frac{3K_1+G_1}{K_1+2G_1}\right]^2 \phi_1\eta_2 + 5G_1\left[\frac{2K_1+3G_1}{(K_1+2G_1)^2}\right]\phi_1\zeta_2 \right\}}{1 - \mu\phi_2 - \frac{2\kappa\mu G_1}{3(K_1+2G_1)}\phi_1\zeta_2 - \frac{\mu^2}{6}\left\{ \left[\frac{3K_1+G_1}{K_1+2G_1}\right]^2 \phi_1\eta_2 + 5G_1\left[\frac{2K_1+3G_1}{(K_1+2G_1)^2}\right]\phi_1\zeta_2 \right\}} \right) \quad (5)$$

where

$$\kappa = \frac{K_2 - K_1}{K_2 + \frac{4G_1}{3}} \quad (6)$$

$$\mu = \frac{G_2 - G_1}{G_2 + G_1\left[\frac{9K_1+8G_1}{6(K_1+2G_1)}\right]} \quad (7)$$

The 3-point parameters ζ_2 and η_2 are given by three-fold integrals depending on the volume fraction of the spheres, ϕ_2, and 2-point and 3-point probability functions. They have been numerically calculated for different spherical assemblies (e.g., random, fcc, bcc, poly- and monodisperse, overlapping and impenetrable) as a function of ϕ_2 [15].

The isotropic stiffness tensor of the mineralized matrix, $\mathbf{C}_M$, is trivially constructed from the moduli K_M and G_M:

$$\mathbf{C}_M = 2G_M\mathbf{I} + \left(K_M - \frac{2}{3}G_M\right)\mathbf{1}\otimes\mathbf{1} \quad (8)$$

where $\mathbf{1}$ is the second-order identity tensor.

Finally, the bulk tissue of a mineralized chitin-protein plane (without pore canals) is modeled as an unidirectional transversely isotropic fiber composite with hexagonal arrangement of the fibers (Fig. 2, IV). The effective stiffness tensor of the ply, $\mathbf{C}_P$, depends on $\mathbf{C}_F$ (Eq. (2)) and $\mathbf{C}_M$ (Eq. (8)). We use the Mori-

Tanaka model to find $\mathbf{C}_P$:

$$\mathbf{C}_P = \mathbf{C}_M + \phi_F[(\mathbf{C}_F - \mathbf{C}_M):\mathbf{A}_F][(1-\phi_F)\mathbf{I} + \phi_F\mathbf{A}_F]^{-1} \quad (9)$$

where

$$\mathbf{A}_F = [\mathbf{I} + \mathbf{S}_F:(\mathbf{C}_M)^{-1}:(\mathbf{C}_F - \mathbf{C}_M)]^{-1} \quad (10)$$

is the strain concentration factor for a chitin-protein fibril in a mineral-protein matrix; $\mathbf{S}_F$ is the corresponding Eshelby's tensor; ϕ_F is the volume fraction of the chitin-protein fibrils.

FFT-based spectral method for the macroscopic scale

For computing the elastic response of the cuticle at the macroscale (see Fig. 2, V), we use a spectral method based on Fast Fourier Transforms (FFT) [11–13] instead of the standard Finite Element Method (FEM). Compared to FEM, the FFT-based method is computationally more efficient and better adapted for periodic materials. Unlike the FEM, it does not require mesh generation prior to finding the solution of a particular boundary value problem.

The FFT-based method is conceived for periodic unit cells, which are discretized by means of a regular 3D grid $\{x\}$ of voxels. In turn, this partition of Cartesian space determines a corresponding grid of the same size in Fourier space $\{k\}$. The iterative algorithm described below is taken from [11] and is based on the use of a homogeneous reference medium of stiffness $\mathbf{C}^0$ that allows to rewrite the local constitutive equations, $\sigma(\mathbf{x}) = \mathbf{C}(\mathbf{x}):\varepsilon(\mathbf{x})$, as:

$$\sigma(\mathbf{x}) = \mathbf{C}^0:\varepsilon(\mathbf{x}) + \tau(\mathbf{x}) \quad (11)$$

where $\sigma(\mathbf{x})$, $\varepsilon(\mathbf{x})$, and $\tau(\mathbf{x})$ are the local stress, strain and polarization tensors, respectively. The polarization field

$$\tau(\mathbf{x}) = \left(\mathbf{C}(\mathbf{x}) - \mathbf{C}^0\right):\varepsilon(\mathbf{x}) \quad (12)$$

is a function of the periodic heterogeneity in terms of the elastic properties, and a current guess of the total strain field.

Enforcing equilibrium, $\sigma_{ij,j}(\mathbf{x}) = 0$, and using the definition $\varepsilon_{kl}(\mathbf{x}) = (u_{k,l}(\mathbf{x}) - u_{l,k}(\mathbf{x}))/2$ where $u_k(\mathbf{x})$ is the displacement field, from Eq. (11) the following system of differential equations is obtained:

$$C^0_{ijkl}u_{k,lj}(\mathbf{x}) + \tau_{ij,j}(\mathbf{x}) = 0 \quad (13)$$

The Green's function method is used to solve the system Eq. (13). It consists in writing the following auxiliary problem:

$$C^0_{ijkl}G_{km,lj}(\mathbf{x} - \mathbf{x}') + \delta_{im}\delta(\mathbf{x} - \mathbf{x}') = 0 \quad (14)$$

where $G_{km}(\mathbf{x})$ is the Green's function associated with the dispacement field, δ_{im} is the Kronecker's delta tensor, $\delta(\mathbf{x})$ is the Dirac delta function and $\mathbf{x}'$ is a constant. Once $G_{km}(\mathbf{x})$ has been determined, the solution of Eq. (13) can be obtained for any function $\tau_{ij}(\mathbf{x})$ from:

$$u_k(\mathbf{x}) = \int_{R^3} G_{ki,j}(\mathbf{x} - \mathbf{x}')\tau_{ij}(\mathbf{x}')d\mathbf{x}' \quad (15)$$

Expressing this convolution integral in Fourier space yields:

$$\widehat{u}_{i,j}(\mathbf{k}) = \widehat{\Gamma}_{ijkl}(\mathbf{k})\widehat{\tau}_{kl}(\mathbf{k}) \quad \text{for} \quad \mathbf{k} \neq 0, \quad \text{and} \quad \widehat{u}_{i,j}(\mathbf{0}) = E_{ij} \quad (16)$$

where $(\widehat{f})$ denotes the Fourier transform of (f), $\Gamma_{ijkl} = G_{ik,jl}$, and E_{ij} is the macroscopic strain applied to the unit cell. The operators in Eqs. (14) and (15) are calculated in Fourier space. Anti-transforming and symmetrizing Eq. (16) yields a new guess for the total strain field, $\varepsilon(\mathbf{x})$, which in turn is used in Eq. (12) to obtain a new guess for $\tau(\mathbf{x})$. The iterative loop is repeated until the input strain field coincides with the output field within a certain tolerance.

RESULTS AND DISCUSSION

The naturally wet cuticle exhibits nonlinear viscoelastic-viscoplastic behavior [8]. Here we consider dry cuticle. After drying, the cuticle becomes linear elastic material and has higher stiffness compared to the wet state but cannot sustain plastic deformations [8]. However, it is better suited for analysis of the substructures Fig. 2, III(a), III(b), IV using nanoindentation data which are reliable only for dry cuticle. Moreover, our modeling is strictly valid for composites with linear elastic components which makes the dry cuticle a good choice for validation purposes.

In Voigt notation, the stiffness tensor of α-chitin obtained from *ab initio* calculations reads [4]:

$$\mathbf{C}_{CH} = \begin{bmatrix} 28 & 2 & 0.1 & 0 & 0 & 0 \\ 2 & 24 & 1.1 & 0 & 0 & 0 \\ 0.1 & 1.1 & 119 & 0 & 0 & 0 \\ 0 & 0 & 0 & 8 & 0 & 0 \\ 0 & 0 & 0 & 0 & 2 & 0 \\ 0 & 0 & 0 & 0 & 0 & 5 \end{bmatrix} \text{GPa} \quad (17)$$

It is defined in a local Cartesian coordinate frame; the vectors of the orthorhombic unit cell a, b, c are along the axes 1, 2, 3, respectively. From Eq. (17) it is seen that α-chitin is strongly anisotropic. The crystal modulus along the chitin chains (c-axis) is determinated by strong covalent bonds. Along the directions a and b, a network of weak hydrogen bonds ensures the cohesion of the chitin chains. Consequently, the elastic constant $(C_{CH})_{33}$ along the c-direction is almost five times larger compared to $(C_{CH})_{11}$ and $(C_{CH})_{22}$ associated with deformations along the a and b directions.

As virtually all cuticle proteins have unknown atomic structure and mechanical properties, they are assumed to be isotropic media and are identified via combined approach using (continuum-scale) modeling and experimental data. The protein properties in the chitin-protein fibrils (Fig. 2, III(a)) are assumed to be the same as in a dry chitin-protein abdominal membrane of lobster reported in [7]. Using microtensile experimental data from [7] and Mori-Tanaka modeling for the membrane, we obtain the Young's modulus of the fibril protein as $E_{FP} = 56\,\text{MPa}$; the experimentally measured Poisson's ratio is $\nu_{FP} = 0.28$ [7]. The stiffness tensor $\mathbf{C}_{FP}$ is then trivially constructed from E_{FP} and ν_{FP}. The ratio length/diameter of the chitin nanofibrils needed to compute the Eshelby's tensor in Eq. (2) is 100, as observed. The volume fraction of chitin in the fibrils is $\phi_{CH} = 0.31$, obtained from measurements of the diameters of the fibrils (5.4 nm [9]) and the chitin nanorods (3 nm). The stiffness, $\mathbf{C}_F$, of the composite fibril is obtained with Eqs. (2) and (3).

In the mineral-protein matrix (Fig. 2, III(b)), the Young's modulus and the Poisson's ratio of the protein are identified as $E_1 = 570\,\text{MPa}$ and $\nu_1 = 0.28$, respectively; those of the ACC spherules are $E_2 = 37\,\text{GPa}$ and $\nu_2 = 0.35$ [20], respectively. The corresponding shear and bulk moduli are: $G_1 = 0.223\,\text{GPa}$, $G_2 = 13.7\,\text{GPa}$, $K_1 = 0.432\,\text{GPa}$, $K_2 = 41.1\,\text{GPa}$. The volume fraction of the ACC spherules, ϕ_2, is obtained using thermo-gravimetric analysis. After converting the weight- to volume fractions and taking into account that the mineral is excluded from the fibrils, we obtain $\phi_2 \approx 0.9$. We choose a microstructure that can accommodate such a high volume fraction of spherical particles, namely that of overlapping spheres. The corresponding 3-point correlation parameters are $\zeta_2 = 0.56$ and $\eta_2 = 0.66$ [15]. The stiffness tensor of the mineralized matrix, $\mathbf{C}_M$, is calculated with Eqs. (4-8).

The bulk tissue of the mineralized chitin-protein planes (Fig. 2, IV) is modeled as a regular hexagonal array of fibrils with (anisotropic) stiffness $\mathbf{C}_F$ embedded in a matrix with (isotropic) stiffness $\mathbf{C}_M$. The fibrils are assumed infinitely long. Their volume fraction, $\phi_F = 0.22$, is obtained from the average fibril diameter (5.4 nm), and the center-to-center distance (11 nm) measured from SEM micrographs. The stiffness tensor $\mathbf{C}_P$ is obtained with Eqs. (9) and (10).

We assume that all dry proteins in the cuticle have Poisson's ratio of $\nu = 0.28$ (as measured in lobster membrane [7]). This leaves the Young's modulus, E_1, of the matrix protein as a 'free' parameter estimated via combined modeling-experimental approach. We identify the above mentioned value of E_1 to be 570 MPa using the nanoindentation data in Fig. 3 obtained from dry endocuticle of lobster claw [7].

In Fig. 3 the Young's modulus obtained from nanoindentation is plotted against the angle between the indented sample surface and the chitin-protein fibrils axis. The experimental data are given by their mean value and the averaged minimum and maximum values of the Young's modulus. The original data points are shown in the insert. It is seen that the Young's modulus along the chitin fibrils is $\sim 60\,\%$ larger compared the modulus in direction perpendicular to the fibrils and the model reproduces the experimental data quite well. Therefore, the presence of chitin fibrils considerably reinforces the mineralized planes along the fibril direction. Because of the twisted plywood structure, at the macroscopic scale the cuticle has in-plane isotropic stiffness enhanced by the presence of the chitin fibrils.

A single mineralized chitin-protein plane without pore canals with fibrils oriented along the Y axis in Fig. 4 has the following stiffness tensor:

$$\mathbf{C}_P = \begin{bmatrix} 9.6 & 3.1 & 3.1 & 0 & 0 & 0 \\ 3.1 & 14.4 & 3.1 & 0 & 0 & 0 \\ 3.1 & 3.1 & 9.6 & 0 & 0 & 0 \\ 0 & 0 & 0 & 3.8 & 0 & 0 \\ 0 & 0 & 0 & 0 & 3.2 & 0 \\ 0 & 0 & 0 & 0 & 0 & 3.8 \end{bmatrix} \text{GPa} \qquad (18)$$

At the macroscale, we construct the periodic RVE geometry of the endocuticle using information from SEM micrographs (Fig. 4, a). The unit cell is for regular hexagonal array of pore canals.

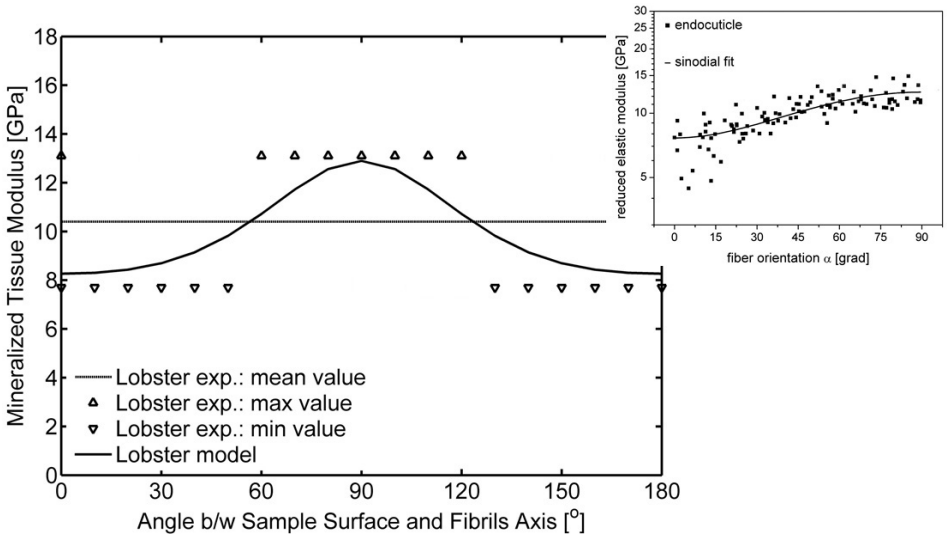

Fig. 3. Mesoscale Young's modulus of lobster endocuticle as a function of the angle between the sample surface (subjected to nanoindentation) and the fibrils axis. Symbols and horizontal line: nanoindentation data, solid line: model predictions. Insert is taken from [7], the original data are plotted for fibril angles from 0° to 90°; solid line in the insert is a fit not related to our model.

For the model set-up and subsequent FFT-based simulations we use the integrated simulation tool DAMASK [12, 13]. The RVE contains $64 \times 110 \times 700 \sim 4.9$ Mio voxels. The twisted plywood is discretized in 100 chitin-protein planes. The pore canals in the RVE are with ellipsoidal cross section (with the ellipse major axis oriented along the fibril direction) and rotate along the Z axis together with the fibrils in the planes (see Fig. 2, V). The rotation angle from bottom to top plate of the RVE is 180°. The area fraction of the pore canals is 36 %; the major/minor axes ratio of the pores ellipsoidal cross-section is 3.5. To avoid convergence problems, the pore canals are filled with perfectly compressible substance with negligible stiffness.

Experimentally, the dry endocuticle from lobster claws subjected to in-plane tension exhibits linear elastic behavior with in-plane Young's modulus ranging from 5.8 to 7 GPa [8]. The cuticle abruptly breaks at deformation of ~ 0.7 % [8]. To analyze the stress-

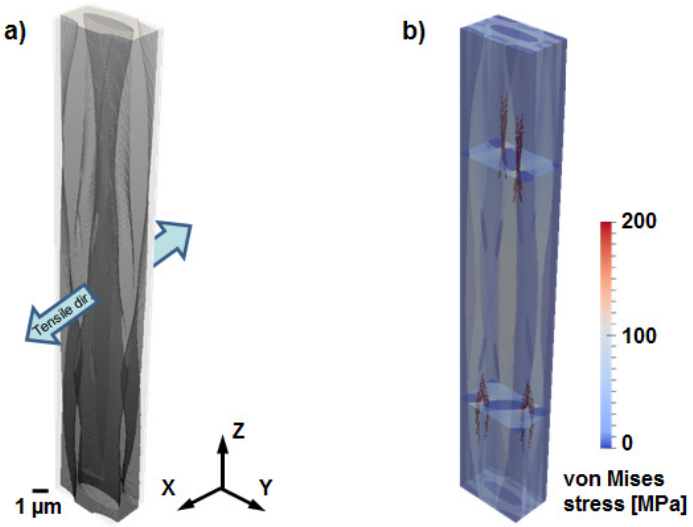

Fig. 4. a) RVE of lobster endocuticle used for FFT-based calculations; b) Stress field map for tensile experiment.

strain state of the cuticle just before failure, we apply tensile strain of 0.7 % to the RVE along the X axis in Fig. 4. The resulting 3D stress field is represented by von Mises stress field map in Fig. 4, b.

We examine the regions where stress concentrations occur because they are the most likely sites for damage initiation before failure. In the stress field map, the highlighted voxels represent stress concentration regions having von Mises stress greater than 154 MPa (the sample stress at failure ranges from 40.1 to 48.8 MPa [8]). It is seen that the stress concentration regions do not span across the whole cuticle thickness (this would strongly decrease its resistance to fracture) but are localized in certain layers with particular orientations of the ellipsoidal pores with respect to the loading direction. This is due to the specific twisted plywood architecture and the ellipsoidal pore shape.

In the pair of highlighted critical planes with highest stress concentrations, one observes that: (i) the major axes of the ellipsoidal pores (as well as the chitin-protein fibrils) are oriented at about $\pm 45^\circ$ w.r.t. the loading direction, (ii) the separation regions between the pores are thinnest, and (iii) the shear stresses in the thinnest separation regions are close to their maximum values (theoretically found at $\pm 45^\circ$ w.r.t. the loading direction). We suggest that these are the necessary conditions for damage initiation in the lobster cuticle.

CONCLUSIONS

We developed an integrated multiscale approach for modeling the elastic properties of biological organic-inorganic nanocomposites that combines three different modeling methods: ab-initio calculations at the nanoscale, homogenization at the mesoscale and FFT-based calculations at the macroscale. The concept is applied to the cuticle of lobster.

At the mesoscale, the properties of cuticle proteins are identified and the bulk mineralized tissue is investigated. The model confirms the experimental nanoindentation data that the Young's modulus of the bulk tissue along the chitin fibrils is $\sim 60\,\%$ larger compared the modulus in direction perpendicular to the fibrils.

At the macroscale, it is found that the highest stress concentrations in the cuticle in uniaxial in-plane loadings are in planes where: (i) the major axes of the ellipsoidal pores (as well as the chitin-protein fibrils) are oriented at about $\pm 45^\circ$ w.r.t. the loading direction, (ii) the separation regions between the pores are thinnest, and (iii) the shear stresses in the thinnest separation regions are close to their maximum values. We suggest that these are the necessary conditions for damage initiation in the lobster cuticle.

The presented approach is general and can be specialized for other organic-inorganic composites like bone, shells, etc. It can also be useful for design and optimization of new biomimetic nanocomposites.

Acknowledgements. *The authors gratefully acknowledge the financial support through the DFG priority program SPP 1420 funded by the Deutsche Forschungsgemeinschaft (German Research Foundation). S.N. is grateful to Dr. D. Ma and Dr. M. Diehl for the help in setting up the FFT 3D model in DAMASK, and to Dr. C. Sachs for providing his thesis.*

REFERENCES

[1] M. F. Ashby, and U. G. K. Wegst, *Phil. Mag.* **84**, 2167–2181 (2004).

[2] P. Fratzl, and R. Weinkamer, *Prog. Mater. Sci.* **52**, 1263–1334 (2007).

[3] M. J. Buehler, S. Keten, and T. Ackbarow, *Prog. Mater. Sci.* **53**, 1101–1241 (2008).

[4] S. Nikolov, H. Fabritius, M. Petrov, M. Friák, L. Lymperakis, C. Sachs, D. Raabe, and J. Neugebauer, *J. Mech. Behav. Biomed. Mater.* **4**, 129–145 (2011).

[5] H. D. Espinosa, J. E. Rim, F. Barthelat, and M. J. Buehler, *Prog. Mater. Sci.* **54**, 1059–1100 (2009).

[6] T. H. P. Harvey, and N. G. Butterfield, *Nature* **452**, 868–871 (2008).

[7] C. Sachs, *Microstructure and mechanical properties of the exoskeleton of the lobster Homarus americanus as an example of a biological composite material*, PhD Thesis, RWTH Aachen, (2008).

[8] H. Fabritius, C. Sachs, P. Romano, and D. Raabe, *Adv. Mater.* **21**, 391–400 (2009).

[9] A. Al-Sawalmih, C. Li, S. Siegel, P. Fratzl, and O. Paris, *Adv. Mater.* **21**, 4011–4015 (2009).

[10] E. Atkins, "Conformations in polysaccharides and complex carbohydrates" in *Proc. Int. Symp. Biomol. Struct. Interactions, Supp. J. Biosci.* **8**, Printed in India, 1985, pp. 375–387.

[11] B. S. Anglin, R. A. Lebensohn, and A. D. Rollett, *Comput. Mater. Sci.* **87**, 209–217 (2014).

[12] F. Roters, P. Eisenlohr, C. Kords, D. D. Tjahjanto, M. Diehl, and D. Raabe, "DAMASK: the Düsseldorf Advanced MAterial Simulation Kit for studying crystal plasticity using an FE based or a spectral numerical solver" in *IUTAM Symposium on Linking Scales in Computations: From Microstructure to Macro-scale Properties* (Pensacola, FL, USA, 17–19 May, 2011), *Procedia IUTAM* **3**, 2012, pp. 3–10.

[13] http://damask.mpie.de/

[14] R. Minke, and J. Backwell, *J. Mol. Biol.* **120**, 167–181 (1978).

[15] S. Torquato, *Random Heterogeneous Materials: Microstructure and Macroscopic Properties*, Springer, New York, 2002.

[16] S. Torquato, *J. Mech. Phys. Solids* **45**, 1421–1448 (1997).

[17] S. Torquato, *J. Mech. Phys. Solids* **46**, 1411–1440 (1998).

[18] T. Mori, and K. Tanaka, *Acta Metall.* **21**, 571–574 (1973).

[19] Y. Benveniste, *Mech. Mater.* **6**, 147–157 (1987).

[20] M. Faatz, W. Cheng, and G. Wegner, *Langmuir* **21**, 6666–6668 (2005).

КОНСТРУКТИВНИ ПРИНЦИПИ И МЕХАНИЧНИ СВОЙСТВА НА БИОЛОГИЧНИ НАНОКОМПОЗИТИ С ЙЕРАРХИЧНА СТРУКТУРА: МНОГОМАЩАБНО МОДЕЛИРАНЕ НА ЧЕРУПКАТА НА ОМАРА Homarus americanus

Св. Николов[1], Х. Фабрициус[2], М. Фриак[2], Д. Раабе[2]

[1] *Институт по механика, Българска академия на науките, ул. "Акад. Г. Бончев" блок 4, 1113 София, България*
[2] *Max-Planck-Institut für Eisenforschung, Max-Planck-Str. 1, 40237 Düsseldorf, Германия*

(Резюме)

От гледна точка на материалознанието, естествените материали чиято основна функция е запазването на устойчиви на механични натоварвания структура и форма (напр. кости, външни скелети) представляват нанокомпозити с йерархична структура, състоящи се от органични и неорганични съставки. Въпреки че съставните компоненти на тези материали имат доста скромни механични свойства, нанокомпозитната тъкан притежава изключителна здравина отнесена към единица плътност. Разбирането на основните конструктивни принципи на естествените органични/неорганични нанокомпозити е от фундаментално и практично значение което би довело до създаването на ново поколение нанокомпозити с изключителни механични свойства.

В тази работа ние комбинираме атомистично моделиране основано на квантовата механика с хомогенизационни методи за моделиране на хетерогенни материали за да получим макроскопичните еластични свойства на черупката на Американския червен омар. Този материал (както и външните скелети на 90% от живите същества на Земята) се състои от хитин, протеини, наноскопични частици от калциев карбонат и вода. Нашият подход е последователно моделиране на механичните свойства от нано- към макро ниво и демонстрира как механичните свойства на черупката се променят и оптимизират с всяко следващо възходящо ниво на йерархичната структура. Предсказаните стойности за модула на еластичност и коефициента на Поасон на черупката са сравнени с данните получени от експерименти. Показано е как от силно анизотропен материал с неподходящи механични свойства на нано-ниво, черупката се превръща в почти изотропен нанокомпозит с отлично отношение здравина/плътност благодарение на "интелигентната" йерархична структура.

1. S. Nikolov, M. Petrov, L. Lymperakis, M. Friák, C. Sachs, H.-O. Fabritius, D. Raabe, and J. Neugebauer, Advanced Materials 22 (2010) 519-526.